RESEARCH ARTICLE



Macrophage depletion increases target specificity of bone-targeted nanoparticles

Marian A. Ackun-Farmmer^{1,2} | Baixue Xiao^{1,2} | Maureen R. Newman^{1,2} | Danielle S.W. Benoit^{1,2,3,4}

²Department of Orthopaedics and Center for Musculoskeletal Research, University of Rochester Medical Center, Rochester, New York, USA

³Department of Chemical Engineering, University of Rochester, Rochester, New York, USA

⁴University of Rochester, Materials Science Program, Rochester, New York, USA

Correspondence

Danielle S.W. Benoit, University of Rochester, Department of Biomedical Engineering, Rochester, New York, USA. Email: benoit@bme.rochester.edu

Funding information

Drug Discovery Grant; National Institutes of Health, Grant/Award Numbers: F31 CA228391, P30 AR069655, R01 AR056696, R01 AR064200; National Science Foundation Career Award, Grant/Award Number: CBET1450987; University of Rochester CTSA award number, Grant/Award Number: UL1 TR002001; University Research Award

Abstract

Despite efforts to achieve tissue selectivity, the majority of systemically administered drug delivery systems (DDSs) are cleared by the mononuclear phagocyte system (MPS) before reaching target tissues regardless of disease or injury pathology. Previously, we showed that while tartrate-resistant acid phosphatase (TRAP) binding peptide (TBP)-targeted polymeric nanoparticles (TBP-NP) delivering a bone regenerative Wnt agonist improved NP fracture accumulation and expedited healing compared with controls, there was also significant MPS accumulation. Here we show that TBP-NPs are taken up by liver, spleen, lung, and bone marrow macrophages (M ϕ), with 76 ± 4%, 49 ± 11%, 27 ± 9%, and 92 ± 5% of tissue-specific Mφ positive for NP, respectively. Clodronate liposomes (CLO) significantly depleted liver and spleen Mφ, resulting in 1.8-fold and 3-fold lower liver and spleen and 1.3-fold and 1.6-fold greater fracture and naïve femur accumulation of TBP-NP. Interestingly, depletion and saturation of MPS using 10-fold greater TBP-NP doses also resulted in significantly higher TBP-NP accumulation at lungs and kidneys, potentially through compensatory clearance mechanisms. The higher NP dose resulted in greater TBP-NP accumulation at naïve bone tissue; however, other MPS tissues (i.e., heart and lungs) exhibited greater TBP-NP accumulation, suggesting uptake by other cell types. Most importantly, neither $M\Phi$ depletion nor saturation strategies improved fracture site selectivity of TBP-NPs, possibly due to a reduction of Mφ-derived osteoclasts, which deposit the TRAP epitope. Altogether, these data support that MPS-mediated clearance is a key obstacle in robust and selective fracture accumulation for systemically administered bone-targeted DDS and motivates the development of more sophisticated approaches to further improve fracture selectivity of DDS.

KEYWORDS

biodistribution, bone targeting, clodronate-liposomes, macrophages, nanoparticles

1 | INTRODUCTION

Drug delivery systems (DDSs) improve solubility, mitigate degradation, and overcome rapid renal excretion of drugs. ^{1,2} Since regulatory approval of Doxil in 1995, 28 nanoparticle (NP)-based DDS have been approved to treat myriad diseases. ³ Despite these successes, an average of only 0.7% of injected DDS dose reaches the tissues of interest. ^{4,5}

To improve tissue specific localization of DDS, active targeting of DDS via introduction of targeting ligands (e.g., peptide, antibody, small molecule, carbohydrate, etc.) has emerged as the next generation of DDSs. However, targeted DDSs suffer from similar systemic delivery challenges to their untargeted counterparts, which has resulted in only modest improvement in target tissue delivery to approximately 0.9% of injected dose. A.5 The marginal success of DDS at achieving tissue

¹Department of Biomedical Engineering, University of Rochester, Rochester, New York, USA

specificity despite longstanding investigations of various DDS designs to improve these parameters (i.e., size, surface charge, shape, surface chemistry, targeting ligands, etc.) suggests that a greater understanding of factors that impact DDS biodistribution is warranted.

Clearance by the mononuclear phagocyte system (MPS) is a barrier to tissue-specific delivery. 1,6 The MPS is comprised of mononuclear cells (i.e., monocytes, neutrophils, dendritic cells) in systemic circulation and within the liver, spleen, lung, lymph nodes, and bone marrow.⁶ Though important for defending the body against foreign substances, the MPS also limits NP-based drug delivery through foreign body recognition and clearance mechanisms. MPS manipulation has been used to improve DDS tissue specific delivery. 7-13 Depleting phagocytic MPS cells including macrophages reduces off-target accumulation of untargeted gold NPs but only provides a slight increase in tumor biodistribution from 0.7% to 2% of injected dose. 8,14 Furthermore, delivery of high doses of DDSs to saturate MPS improves tumor biodistribution by up to 30% of injected dose per tumor weight for liposomes and gold nanoparticles. 15,16 However, neither of these approaches are clinically translatable due to innate immune system manipulation and potential toxicities associated with high doses of DDSs. Rather, these studies highlight the need to overcome MPS clearance to improve DDS efficiency. Notably, the aforementioned studies focused on passive (e.g., untargeted) DDS delivery within tumor models rather than targeted counterparts and other disease indications.

Although MPS is a universal barrier in drug delivery, very little is known about its function in bone delivery despite bone marrow's role as an MPS organ. Considering poor bone biodistribution of systemically administered drugs (<1%)¹⁷ and the economic impact of orthopedic injuries, osteoporosis, and hematologic and bone-metastasizing cancers, improving drug delivery to bone is highly significant. Previously, we developed a bone-targeted DDS that improved bone regeneration owing to robust delivery of a Wnt agonist to fracture sites. 18 Specifically, tartrate-resistant acid phosphatase (TRAP) binding peptides (TBP) were introduced to enable bone targeting 16 of poly(styrene-alt-maleic anhydride)-b-poly(styrene) (PSMA-b-PS) nanoparticles (NPs), which improve drug solubility and stability. 19,20 Notably, there was significant off-target liver and spleen accumulation of TBP-NPs, which limits the potential of this bone-targeting platform. 18 In the current study, liver, spleen, and lung accumulation of TBP-NPs was investigated to identify macrophage involvement in systemic TBP-NP accumulation. Next, macrophage (Mφ) depletion was investigated to improve delivery efficiency of TBP-NPs in both uninjured and fractured mice. Finally, high doses of TBP-NP were used to saturate MPS and evaluate subsequent TBP-NP fracture biodistribution to interrogate the role of MPS in delivery of targeted bone-targeted DDS.

2 | MATERIALS AND METHODS

2.1 | Materials

All chemicals were supplied by Sigma-Aldrich and Alfa Aesar unless stated otherwise and solvents used were spectroscopic grade.

Distilled/deionized water (ddH $_2$ O) with resistivity of 18 M Ω or greater (ultrapure) was used for all studies.

2.2 | Animals

Male C57BL/6J and female BALB/c mice (6 to 8-week-old) from Jackson Laboratories (Bar Harbor, ME) were used for uninjured and fracture studies, respectively, to maintain continuity and enable comparisons with previous studies. Animals were maintained in the University of Rochester Vivarium according to standard housing conditions. Analgesics (0.05 mg/kg buprenorphine [IP]) were provided for pain management throughout fracture study experiments. Anesthesia (60 mg/kg ketamine and 4 mg/kg xylazine [intraperitoneal injection, IP]) was provided during retroorbital injections (5 and 50 mg/kg NPs) and mice were sacrificed using carbon dioxide followed by cervical dislocation. All animal experiments were approved by the University of Rochester Institutional Animal Care and University Committee of Animal Resources (UCAR).

2.3 | Peptide and nanoparticle synthesis, conjugation, and characterization

Peptide synthesis has been detailed previously in the following publications. 18,21,22 Briefly, tartrate-resistant acid phosphatase (TRAP) binding peptides (TBP; sequence: TPLSYLKGLVTVG) were generated using microwave-assisted solid-phase peptide synthesis (CEM Corp, Liberty1 synthesizer) and Fluorenylmethyloxycarbonyl chloride (FMOC)-protected amino acids (AAPPTec and Peptides International). Amino acid coupling was achieved with an activator mix of 0.5 M O-(benzotriazole-1-vl)-N.N. N',N'-tetramethyluronium hexafluorophosphate (HBTU) in DMF and an activator base mix of 2 M N,N-diisopropylethylamine (DIEA) in 1-methyl-2-pyrrolidinone (NMP) while deprotection of amino acids was achieved with 5% piperazine in dimethylformamide (DMF). Cleavage from Fmoc-Gly-Wang resin (Millipore, Massachusetts) was achieved via 92.5% trifluoroacetic acid (TFA), 2.5% H₂O, 2.5% 3,6-dioxa-1,8-ocatanedithiol (DODT), and 2.5% triisopropylsilane (TIPS) for 2.5 hr followed by precipitation in ice-cold diethyl ether. Peptide was vacuum filtered and molecular weight was validated using matrix-assisted laser desorption ionization time-of-flight mass spectrometry (MALDI-TOF; Brüker Autoflex III).

Development of PSMA-*b*-PS based amphiphilic diblock copolymers formed into NPs for these studies has been detailed in previous publications. Briefly, one-pot reversible addition-fragmentation chain transfer agent (RAFT) polymerization was used. Briefly and maleic anhydride recrystallized from chloroform ([STY]:[MA] = 5:1) were added to chain transfer agent, 4-cyano-4-dodecylsulfanyltrithiocarbonyl sulfanyl pentanoic acid (DCT; [STY]:[CTA] = 100:1) and the radical initiator, 2,2'-azo-bis (isobutylnitrile) (AIBN), recrystallized from methanol ([CTA]: [AIBN] = 5:1) in dioxane (50% w/w). Diblocks were analyzed using gel permeation chromatography as previously documented. NPs were formed by dissolving diblock copolymers (200 mg) in DMF (20 ml) and adding ddH₂O (21 ml) via a syringe pump set at

24.4 μ l/min. NPs were dialyzed against ddH $_2$ O for 72 hr using 6–8 kDa MW cut-off dialysis tubing 16-18 (Spectrum Laboratories, California) and filtered using 0.2 μ m cellulose acetate filters (VWR international, Pennsylvania) prior to storage in 4°C. Gravimetric determination of NP concentrations was performed via lyophilization.

Peptide coupling to NPs has been described previously. ^{18,21} Briefly, 1-ethyl-3-(3-dimethylamino)propyl carbodiimide (EDC, Thermo Fisher) ([EDC]:[polymer] = 10:1), 5 mM *N*-hydroxysulfosuccinimide (sulfo-NHS, Thermo Fisher), and TBP ([TBP]:[polymer] = 10:1 in 0.1 M sodium phosphate buffer (pH 7.4)) were combined and mixed overnight. Samples were dialyzed against ddH₂O for 72 hr (MWCO 6-8 kDa) to remove unconjugated peptide and conjugation efficiency was determined using fluoraldehyde o-phthaldialdehyde (OPA, Thermo Fisher, $E_x/E_m = 360 \, \text{nm}/455 \, \text{nm}$) and nanoparticle tracking analysis (NTA, Nanosight NS300). NP physiochemical properties such as size and surface charge were analyzed using dynamic light scattering (DLS) and a Malvern Zetasizer.

2.4 | Femur fracture model

Mid-diaphyseal femur fractures were established as previously detailed. Briefly, an 8 mm skin incision was used to expose the femur midshaft and a fracture was made using a rotary Dremel with a diamond blade attachment. Following fracture, a 25-gauge needle was inserted into the medullary canal to stabilize the femur.

2.5 | Clodronate treatments

PBS and clodronate liposomes (CLO; 5 mg/ml) were purchased from Liposoma BV (Netherlands). Uninjured mice were retro-orbitally injected (100 μ l) every other day for four doses with PBS and CLO. For fracture studies, mice were retro-orbitally injected every other day for three doses prior to fracture and injected 1 day after fracture.

2.6 | Nanoparticle injections and biodistribution

Cy5 or Cy7 amine labeling of TBP-NPs was achieved by mixing molar ratios of EDC, dye, and polymer (10:10:1), 5 mM sulfo-NHS, and 0.1 M sodium phosphate buffer (pH 7.4) overnight. Samples were dialyzed against ddH $_2$ O for 72 hr (MWCO 6–8 kDa) to remove unconjugated dye prior to use. NP physiochemical properties such as size and surface charge were analyzed using dynamic light scattering (DLS) and a Malvern Zetasizer.

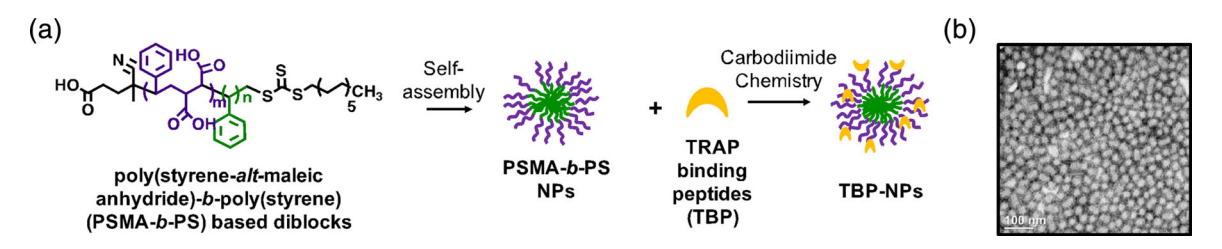
To investigate fracture accumulation of TBP-NPs, 5 mg/kg dose Cy7-TBP-NP, Cy5-TBP-NP, and 50 mg/kg Cy5-TBP-NPs were retroorbitally injected a day after the final dose of PBS or CLO liposomes in uninjured mice and 3 days after fracture in fracture models. ¹⁶ Twenty-four hours following TBP-NP injections, mice were sacrificed, perfused with PBS, and imaged using the XENOGEN/IVIS imaging system (Perkin-Elmer) ($E_x/E_m = 640/800$ for Cy5 and $E_x/E_m = 745/800$ nm for Cy7) quantification of NP biodistribution in anatomized tissues. Free draw contour regions of interest (ROIs) were placed around individual organs to determine the total radiance efficiency (TRE) using Living Image software (Perkin-Elmer). The TRE of each organ was normalized to the sum of TRE to calculate the percent of total TRE for each organ. Control organs from untreated mice were used for background subtractions due to tissue autofluorescence.

2.7 | Tissue processing and immunohistochemistry

Tissues isolated from mice injected with Cy5-TBP-NPs 24 hr prior were stored in neutral buffered formalin (NBF) for 3 days and submerged in a daily sucrose gradient (10, 20, and 30% sucrose in PBS) prior to being embedded in Cryomatrix (Thermo Scientific, Cat #: 6769006) on dry ice. Cryomolds were sectioned using a Leica CM1850 cryostat (Germany) and sections were stored in -20° C prior to staining. To stain F4/80 positive cells in tissue samples, slides were dried in a 37°C oven overnight, fixed in cold acetone (-20°C) for 10 min, and washed three times in phosphate buffered solution (PBS) for 5 min. Sections were then washed twice in ×1 TBS/0.3% Triton X-100 for 5 min. Slides were incubated for 30 minutes at room temperature in blocking solution (10% normal goat serum in PBS, Cat #: 50-062Z) to reduce non-specific primary antibody staining. Primary antibody (Cat #: ab6640) was added to the slide and sample stored in a humidified chamber at 4°C overnight. Slides were washed three times in ×1 TBS/0.3% Triton X-100 for 5 min each and secondary antibody (Cat #: ab150160) was added to the slide in a humidified chamber at room temperature for 30 min protected from light. Samples were washed three times in PBS for 5 min each and then mounted using DAPI containing mounting media (Cat #: ab104139). Slides were imaged using a Nikon A1R HD laser scanning confocal microscope. Quantification was performed using Imaris Image Visualization & Analysis Software (Oxford Instruments).

2.8 | Flow cytometry

Cy5-TBP-NP injected mice were sacrificed 24 hr later, and bone marrow tissue was harvested for cell isolation by flushing with PBS + 2% FBS (FACS buffer) using a 25-gauge needle. Liberated marrow cells were resuspended in 1 mg/ml collagenase type IV (Sigma), 2 mg/ml dispase (Sigma), and 10 U/ml DNase (Thermo Fisher Scientific) dissolved in Hank's Balanced Salt Solution (HBSS) for 45 min at 37°C. Red blood cell (RBC) lysis buffer (156 mM NH₄Cl, 127 µM EDTA, and 12 mM NaHCO₃) was used to lyse RBCs for 5 min at room temperature. Antibody incubations were performed for 30 min on ice in the dark using PE-Cy7 labeled TER-119 (Biolegend, Cat # 116221), PE-labeled CD51 (Thermo Fisher Scientific, Cat #: 12-0512-81), PE-Dazzle 594 labeled CD31 (Biolegend, Cat #: 102429), Brilliant Violet (BV) 510 labeled Ly6G (Biolegend, Cat #: 127633), SuperBright 702 labeled F4/80 (Thermo Fisher Scientific, Cat #: 67-4801-80), BV 785 labeled CD206 (Biolegend, Cat #: 108123), PerCP-Cy5.5 labeled



SCHEMA 1 (a, b) Poly(styrene-*alt*-maleic anhydride)-*b*-poly(styrene) (PSMA-*b*-PS) NP functionalization with TRAP binding peptide (TBP-NPs). Scale bar = 100 nm in b

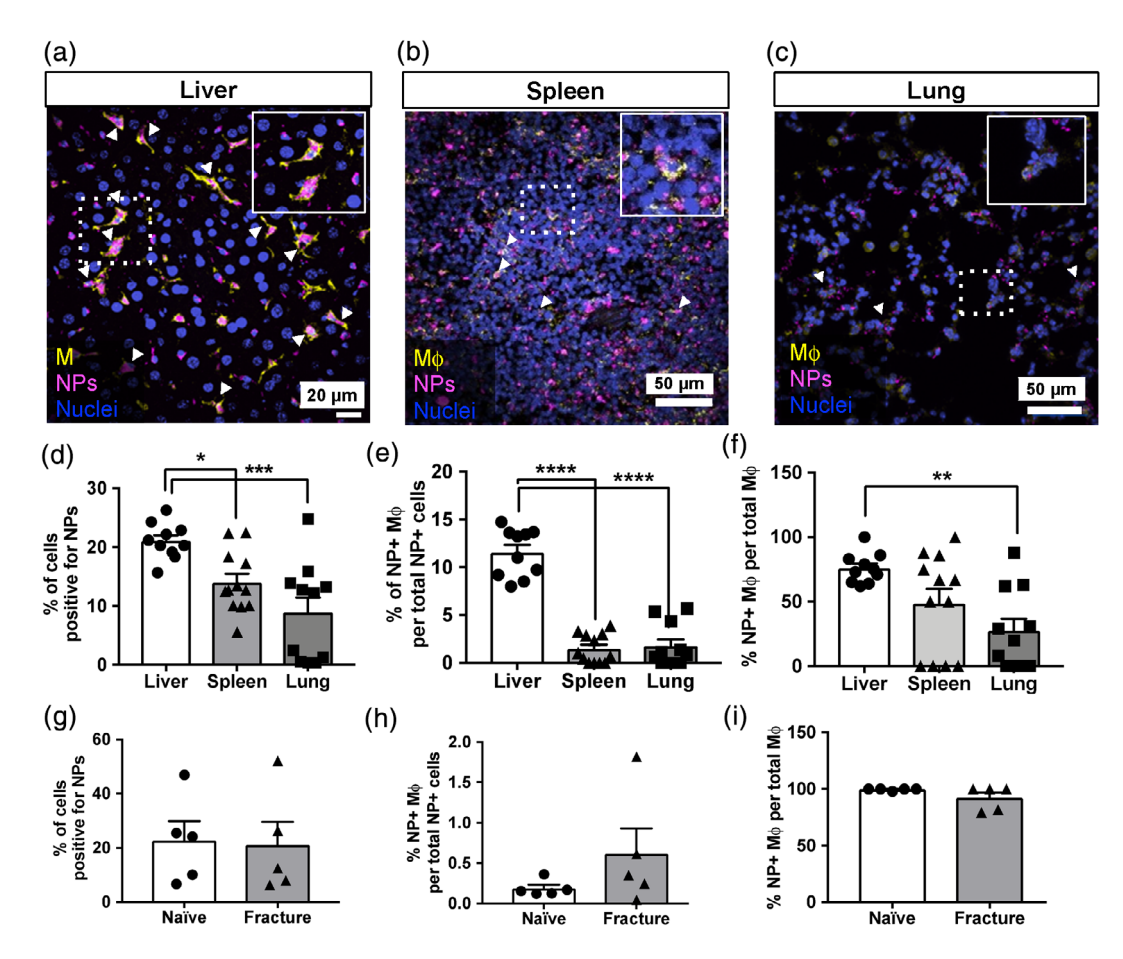
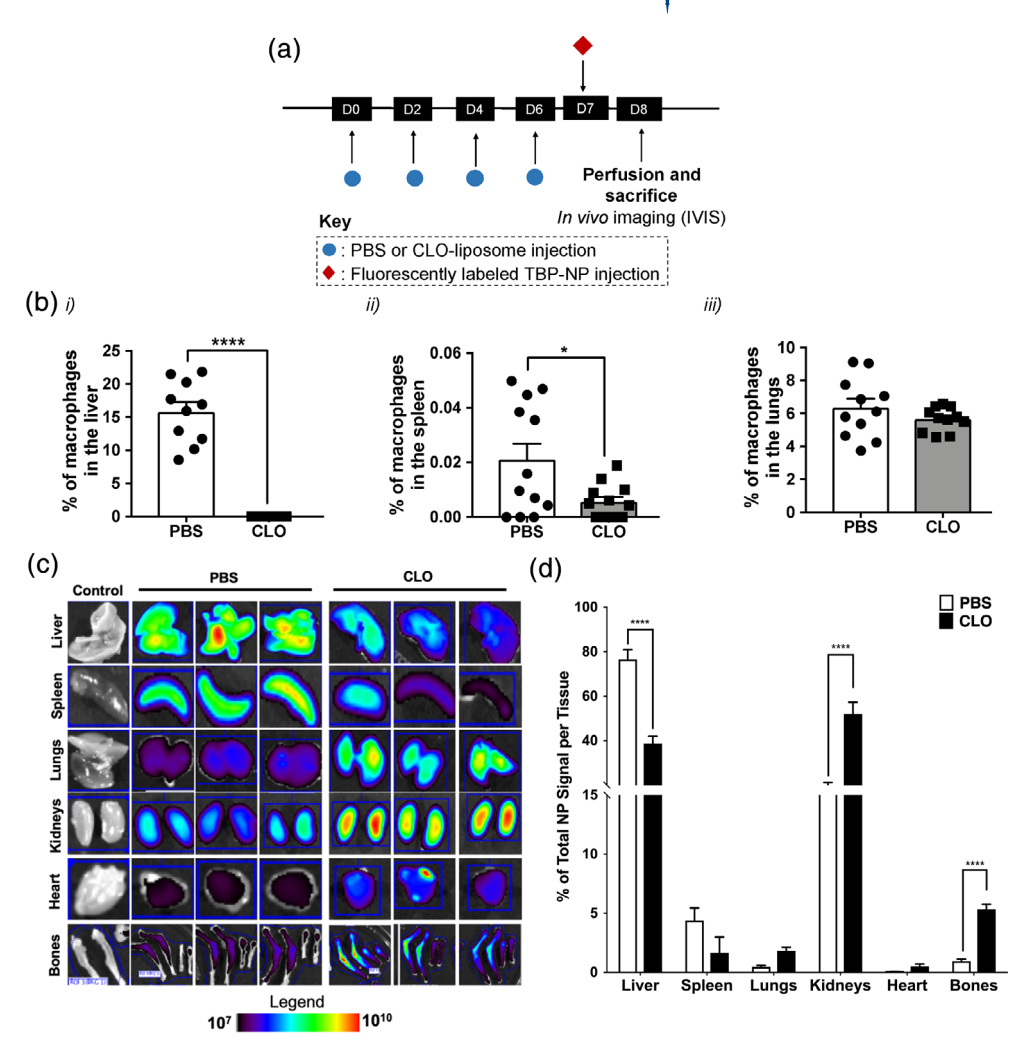


FIGURE 1 M ϕ in the liver, spleen, lungs, and bone take up TBP-NPs. Representative histological images of (a) liver, (b) spleen, and (c) lung. Scale bar: 20 µm (liver). Scale bar: 50 µm (spleen and lung). (d-f) Imaris was used to quantify cell nuclei, NP signal and M ϕ as measured by F4/80 expression. Data represents mean \pm standard error mean (n=5 per group). The part figure (d) shows the % of cells positive for NPs. * p < .05 and **** p < .001 represents significant differences between groups using one-way ANOVA followed by Tukey's multiple comparisons test. The part figure (e) shows the % of F4/80+/NP+ cells. ***** p < .0001 represents difference between groups using one-way ANOVA followed by Tukey's multiple comparisons test. (f) Quantification of the percent of M ϕ positive for NPs. ** p < .01 represents difference between groups using one-way ANOVA followed by Tukey's multiple comparisons test. (g-i) Flow cytometry analysis of M ϕ (CD45+/F4/80+/Gr-1-) in naïve and fractured bone. Data represents mean \pm standard error mean (n = 5)

Ly6A/Ly-6E (Biolegend, Cat #: 108123), and APC-Cy7 labeled CD45 (BD Biosciences, Cat #: 561037). Samples were resuspended in 100 μ l FACS buffer and analyzed on an LSRII flow cytometer: 3 lasers, 355 nm, 488 nm, and 633 nm (BD Biosciences). 74,000–310,000 total events were collected for fractured and unfractured bone, respectively.

In a subset of studies, liver tissue was processed for flow cytometry using 10 ml Roswell Park Memorial Institute 1640 (RPMI 1640, Hyclone) containing 0.1% type IV collagenase, spleen tissue was processed using PBS + 2% FBS containing 10 U/ml DNAse, and lung tissue was digested in HBSS containing 1 mg/ml DNase/5 mg/ml type I collagenase. Briefly, livers were minced, placed in digestion media at

FIGURE 2 Clodronate treatment significantly improved bone accumulation of TBP-NPs in uninjured mice. (a) Timeline showing injection of PBS. clodronate liposomes (CLO), and fluorescently labeled TBP-NPs. (b) Percent of F4/80 positive cells in the liver, spleen, and lung via histological analysis. Data represents mean ± standard error mean (n = 8). *p < .05. **** p < .001 represent differences between groups via unpaired ttests. (c) IVIS images. Bones = femur, tibia, radius, and ulna. (d) Quantification of IVIS images showing the percent of total TBP-NP signal per tissue. Data represents mean ± standard deviation (n = 3). **** p < .001represents comparisons performed using unpaired t-tests between PBS and CLO in uninjured mice



 37° C for 30 min, strained through 70 μm filters after centrifugation, and incubated in RBC lysis buffer for 5 min at 4°C to remove red blood cells. Spleens were crushed through 70 μm cell strainers and into digestion media, incubated at 37° C for 30 min, and incubated in RBC lysis buffer for 5 min at 4° C. Lungs were incubated in digestion media for 30 min at 37° C, tissue was disrupted using a 18-gauge needle, cells were passed through a 70 μm cell strainer prewetted with 0.5% BSA in PBS and incubated in ACK lysis buffer for 5 min at 4° C. All cells were centrifuged at 300g for 5 min at 4° C between digestion, straining, and ACK lysis steps. Cell suspensions were incubated with APC labeled F/480 (eBioscience/17-4801-82/BM8) and 50 μg/ml propidium iodine in FACs buffer for flow cytometry.

2.9 | Statistical analysis

Prism software (GraphPad Version 6.0) was used for all statistical analysis. Comparisons between two groups were performed using unpaired t-tests. Multiple comparisons were performed using one-way or two-way ANOVA followed by Tukey's post-hoc analysis or Dunnett's post-hoc analysis to determine significance (*p*-values are noted in figure legends).

3 | RESULTS

3.1 | MPS cells uptake bone targeted PSMA-*b*-PS NPs

Previous studies that exploited TRAP-binding peptide targeted PSMA-b-PS NPs (TBP-NPs; Schema 1) to deliver small molecule Wnt agonists revealed substantial liver and spleen accumulation despite improved localization at and healing of fractures. 18 Based on this observation, in vivo NP uptake by tissue resident M_{Φ} was investigated 24 hr after TBP-NP injection. Histological analysis of liver, spleen, and lung Mφ revealed robust TBP-NP uptake (Figure 1a-c). Quantification of histological images was performed to identify the percent of total cells positive for NPs, NP positive (NP+) Mφ per total NP+ cells, and NP+ Mφ per total Mφ, as shown in Figure 1d-f. Of all cells analyzed in liver, spleen, and lung, $21 \pm 1\%$, $14 \pm 1\%$, and $9 \pm 2\%$ were positive for NPs, respectively (Figure 1d). Furthermore, of the total NP+ cells in liver, spleen, and lung, $12 \pm 0.8\%$, $1.5 \pm 0.4\%$, and $1.8 \pm 0.7\%$ (Figure 1e) were M ϕ , as measured by analysis of histological sections, suggesting significant NP uptake in $M\phi$ and also non- $M\phi$ cell types. Of all F4/80+ $M\phi$ in the liver, spleen, and lung, 76 \pm 4%, 49 \pm 11%, and 27 \pm 9% were NP+ (Figure 1f). Varying degrees of tissue $M\phi$ uptake corroborate other studies that have

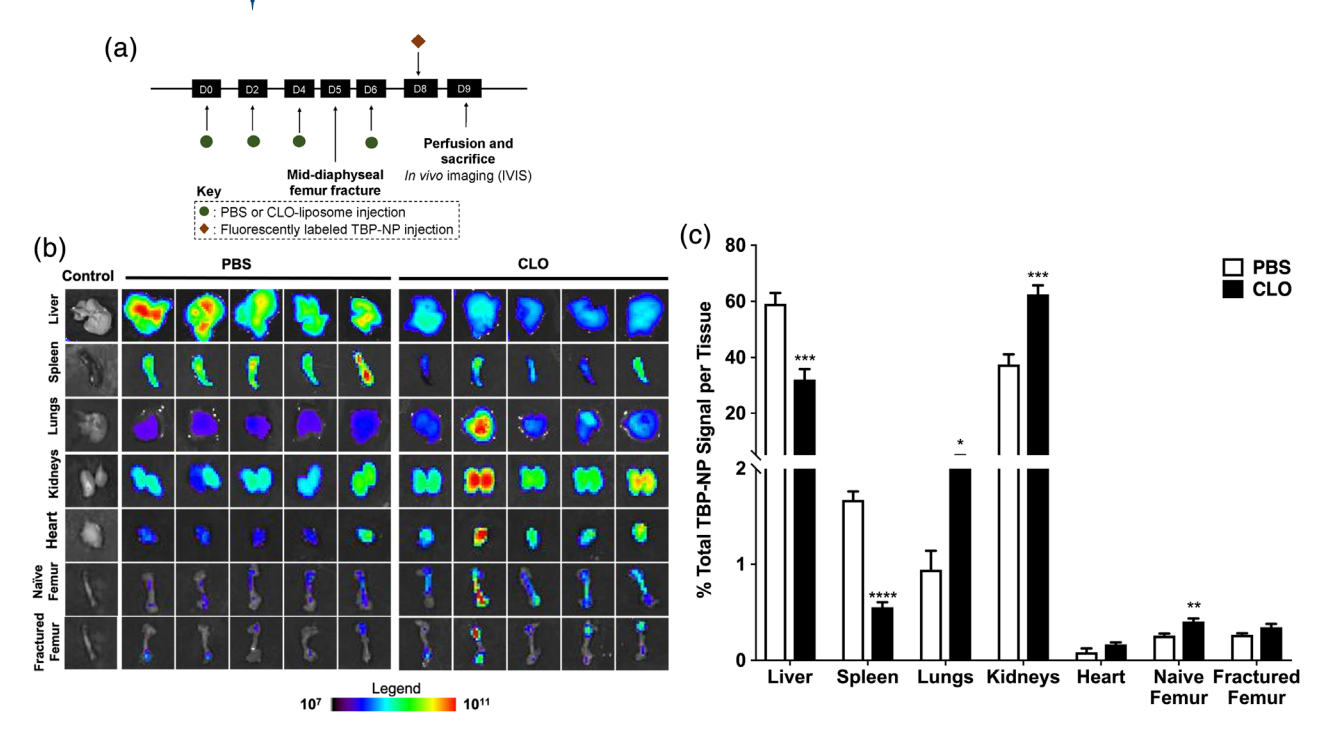


FIGURE 3 Clodronate treatment significantly improved naïve contralateral bone accumulation of TBP-NPs in fractured mice. (a) Timeline of clodronate and NP treatments. (b) IVIS images of tissue after TBP-NPs injection 3 days after fracture. (c) Quantification of IVIS images. Data represents mean \pm standard error mean (n = 5). * p < .05, ** p < .01, *** p < .001, and **** p < .0001 represents statistical differences noted using unpaired t-tests between PBS and CLO mice

shown that liver resident Mφ, known as Kupffer cells, are primarily responsible for systemically administered NP clearance, followed by splenic Mφ and, to a lesser extent, lung Mφ. ⁶ Since the intention of TBP-NP is to deliver drugs to bone, cellular uptake of NPs in naïve and fractured femurs was also quantified. There were no differences in the percent of cells positive for NPs, Mφ per total NP+ cells, and NP+ Mφ per total M_{\phi} between na\(\text{ive} \) and fractured femurs (23 ± 7% and 21 ± 9%; Figure 1g-i). Of the total NP+ cells isolated from naïve and fractured bone, $0.19 \pm 0.04\%$ and $0.6 \pm 0.3\%$ were M ϕ , suggesting involvement of other cells besides Mφ in TBP-NP uptake (Figure 1h). Of total M ϕ from naïve bone and fractures, 99.6 ± 0.4% and 92 ± 5% were NP+, respectively, highlighting that Mφ are highly phagocytic of TBP-NPs even at the target tissue (Figure 1i). Of note, neutrophils, osteoblasts, and endothelial cells at naïve and fractured bone were also observed to be NP+ (Figure S3). Overall, this study showed that Mφ within MPS tissue play a major role in clearance of systemically injected bone-targeted NPs and are also responsible for significant NP uptake at the target site.

3.2 | Systemically depleting $M\phi$ improves bone accumulation

Based on data showing that M ϕ play a significant role in bone-targeted PSMA-*b*-PS NP clearance (Figure 1), we postulated that M ϕ depletion would improve bone targeting efficiency. Clodronate liposomes (CLO) were injected every other day for four total doses to systemically deplete M ϕ prior to TBP-NP injection (Figure 2a).²⁴ Qualitative histological analysis performed 48 hr after the final CLO

dose showed nearly complete loss of M\phi in the liver (Figure 2b), which was corroborated via flow cytometry analysis showing a significant reduction of 52% Mφ (Figure S2). In the spleen and lung, flow cytometry of Mo corroborated histology that showed a decrease in spleen $M\phi$ and no difference in lung $M\phi$ (Figure S2). After CLO $M\phi$ depletion, NPs were injected into uninjured mice (Figure 2a). Twentyfour hours after CLO treatment, in vivo live imaging system (IVIS) analysis revealed a significant 5.6-fold increase in integrated NP signal within the collected bones (tibia, femur, radius, and ulna) of CLO depleted compared with non-depleted mice. In contrast, there was a significant two-fold decrease of NP in liver. Though not statistically significant due to variability, a 2.6-fold reduction of NP was also observed in the spleen (Figure 2c,d). Thus, increased accumulation of TBP-NP at bone and decreases at liver and spleen are consistent with reduced clearance of TBP-NP by Mφ, which maintains greater concentrations of TBP-NP systemically to enable more robust extravasation to bone. However, increases in NP signal were also observed for lungs, heart, and kidney of 4-fold, 7-fold, and 3-fold versus non-depleted mice, indicating a shift in biodistribution due to CLOreduction of Mφ (Figure 2c,d).

3.3 | Depleting Mφ improves bone-targeted NP accumulation in naïve bone but not fractures

With significant improvement in bone biodistribution observed following $M\varphi$ depletion in unfractured mice, NP biodistribution was investigated post-fracture. To ensure that $M\varphi$ would not recover

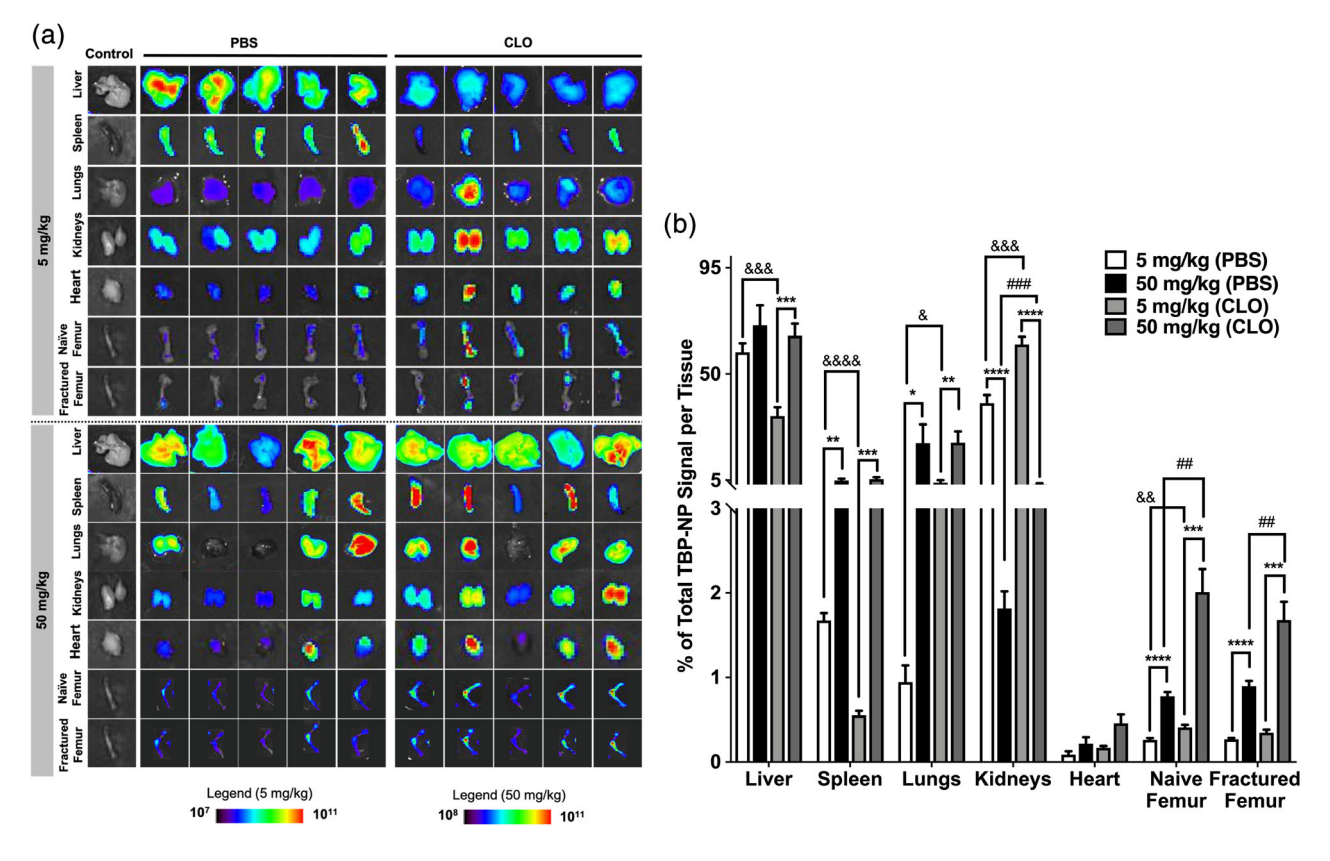


FIGURE 4 NP biodistribution is dose dependent. (a) IVIS images showing the accumulation of TBP-NPs in various tissues after low and high doses in PBS and CLO treated mice. (b) Quantification of TBP-NP accumulation after low and high dose treatments in fractured mice. * p < .05, ** p < .01, **** p < .001, **** p < .001 represents statistical differences noted using one-way ANOVA followed by Tukey's multiple comparisons test. $\frac{\&\&}{V} < .01$, $\frac{\&\&\&\&}{V} < .001$, $\frac{\&\&\&\&}{V} < .001$ represents statistical differences using t-test comparisons between PBS and CLO treated with 5 mg/kg. *#p < .01, *#*p < .001 represents differences between PBS and CLO treated with 50 mg/kg. Data represents mean \pm standard error mean (n = 5)

during the fracture healing process, three CLO injections were administered every other day prior to femur fracture and one dose after fracture (Figure 3a). Three days after fracture, when TRAP deposition is elevated, TBP-NPs were injected, as in previous studies. ¹⁸ Similar to uninjured mice, CLO treatment resulted in a significant decrease of NP signal in the liver by 1.8-fold (Figure 3b) and a 1.7-fold and 4-fold increase in kidney and lung accumulation. However, unlike uninjured mice, there was a significant 3-fold reduction of NP signal in the spleen. Additionally, a significant 1.6-fold increase of TBP-NP was observed in contralateral femurs, while fractures exhibited an insignificant 1.3-fold increase in TBP-NP signal (Figure 3b). Overall, these data suggest that reducing $M\phi$ is an effective way to improve bone accumulation, albeit only for uninjured bone and not fractures.

3.4 | NP dose influences biodistribution via MPS saturation

To test whether MPS could be saturated or overwhelmed to increase bone accumulation, TBP-NP dose was increased from 5 to 50 mg/kg in both clodronate-treated and untreated mice. Data are shown as percent of total tissue signal, resulting in normalization to total dose accumulated in tissues on a per mouse basis. Generally, CLO

treatment at the high dose did not change liver, spleen, or lung accumulation but increased heart, naïve, and fractured femur accumulation 2-fold, 2.6-fold, and 1.9-fold, respectively (Figure 4). However, 50 mg/kg doses resulted in three-fold increases in NP signal in naïve and fractured femurs in non-depleted mice compared with the 5 mg/kg dose (Figure 4a). Interestingly, there were no differences in liver accumulation between the low and high dose treatments in nondepleted mice, suggesting that liver saturation was achieved even at the 5 mg/kg dose (Figure 4b). In other MPS organs, that is, spleen and lungs, there were significant, 2.9-fold and 22-fold increases in accumulation in the high versus low dose in non-depleted mice (Figure 4b). In Mφ depleted mice, greater accumulation was found in the spleen (9.8-fold vs. low dose) but less so in the lungs (5-fold vs. low dose; Figure 4b). Higher doses in Mφ depleted mice resulted in 5-fold increases in both naïve femur and fracture accumulation compared with the low dose, suggesting that combined effects of depleting Μφ and MPS saturation improve tissue selectivity (Figure 4b). Overall, these data demonstrated that high dose TBP-NP combined with reducing Mφ in MPS tissues was an effective method to improve bone accumulation, although these manipulations generally increased overall levels of TBP-NP accumulation irrespective of tissue and did not selectively improve TBP-NP accumulation at fractures compared with uninjured contralateral femurs.

4 | DISCUSSION

Despite initial excitement of the concept of tissue-specific targeting and potential for revolutionary improvements in drug delivery, 25 the development of DDS "magic bullets" remains elusive. Increasingly, evidence shows that MPS clearance hinders efficient DDS-mediated drug delivery irrespective of introduction of tissue-targeting ligands.⁶ Previously, we showed that despite approximately 3.5-fold greater fracture accumulation and expedited fracture healing via Wnt agonist delivery by tartrateresistant acid phosphatase (TRAP) binding peptide (TBP)-targeted PSMAb-PS NPs, substantial off-target accumulation occurs, which may limit further DDS development. 18 Herein, we aimed to investigate the role of MPS in bone-targeted PSMA-b-PS NP accumulation in bone versus offtarget tissues. Clodronate liposomes (CLO) were used to systemically deplete M\(\pha\) in control (uninjured) and fractured mice, leading to a significant reduction in liver accumulation and improved localization at uninjured but not fractured bone. In the lung and kidneys, clodronate treatment significantly increased NP accumulation, while a significant reduction in spleen accumulation was observed but only in fractured mice. Mφ saturation using 10-fold higher doses of TBP-NP in non-depleted and Mo depleted mice also increased fracture accumulation of NP, although this improvement was not specific to fractures versus contralateral femurs. In the liver, spleen, and lung, higher NP doses did not impact accumulation in non-depleted and Mφ depleted mice while NP accumulation was significantly increased in kidneys and heart between non-depleted and Mo depleted mice. Overall, our studies show that M_{Φ} depletion and saturation strategies alter TBP-NP biodistribution but fail to improve fracture targeting, which motivates materials-focused strategies rather than biological manipulation to improve bone targeting.

Similar to tumors, fractured bone is characterized by increased inflammation and vascular permeability during healing, resulting in enhanced permeability and retention (EPR) mediated accumulation of NPs. 18,26 EPR enables DDS escape from systemic circulation via leaky vasculature associated with tumors, injury, and inflammation.²⁷ Nevertheless, EPR does not guarantee tumor accumulation due to MPS clearance mechanisms.^{7,8} Here, the role of MPS was investigated for limiting tissue-specific accumulation of fracture-targeted DDS. Our data show that naïve contralateral bone accumulation of NP was increased in the Mφ depleted fracture model and even more so in the uninjured model, suggesting systemic inflammation and increased vascular permeability due to the fracture resulted in increased overall widespread bone extravasation in conjunction with reduced clearance of TBP-NP. Similarly, CLO reduces MPS uptake of liposomal NPs, silver NPs, silica NPs, and gold NPs, which subsequently increases NP circulation time and improves delivery to tumors.^{7,8} In our studies, increasing NP dose 10-fold in nondepleted fractured mice increased naïve bone accumulation, but did not improve fracture accumulation, similar findings to those in a tumorbearing model.¹⁶ Even combining M_Φ depletion and saturation did not improve selective fracture accumulation compared with naïve bone, which suggests an important role of TRAP in the TBP-NP DDS. While TBP-NPs accumulate passively at fractures due to EPR, TBP binding of TRAP deposited by osteoclasts during resorption results in NP persistence.¹⁸ This may be due to the depletion of Mφ, which are osteoclast

progenitors, subsequently reducing osteoclast-deposited TRAP, as previously described. ^{24,28} These data highlight a limitation of M ϕ depletion in the context of fracture site accumulation of TBP-NPs and motivate other strategies to maintain tissue selectivity while evading M ϕ .

To enable direct comparisons with our previous data, 18,21 and broaden the applicability of these findings, different sex and strain mice were used in our uninjured and fracture models. Interestingly, Mφ depletion in both models resulted in decreased liver and spleen NP accumulation coupled with increased lung, kidney, heart, and naïve bone accumulation. Biodistribution observed in our studies are complementary to others that show DDS accumulation shifts from liver to other MPS organs including lung, kidney, and even lymph nodes after CLO treatment.^{7,8} Similar to our findings, studies in tumor and non-tumor models show CLO-mediated depletion of $M\phi$, which are responsible for DDS clearance after systemic administration.⁶ reduced but did not completely abrogate liver accumulation regardless of DDS or disease pathology. 7,8,11,14,29 Thus, M φ depletion is insufficient to eliminate all liver accumulation, likely due to uptake by residual Mφ as well as hepatocytes. hepatic B cells, and other cells in liver. 29,30 Our studies show that approximately 43% of NP+ cells in the liver were not Mφ, further supporting the notion that other cells in the liver were responsible for NP accumulation. In our studies and others, spleen Mφ were depleted using CLO, yet, unlike tumor studies that use liposomes, gold NPs, and silica NPs, ^{7,8} we observed decreased TBP-NP accumulation in the spleen after CLO treatment, which may suggest differential NP-immune system interactions based on DDS type.31 Conversely, exosomes and polymeric NPs11,14 exhibit reduced spleen accumulation in Mφ depleted non-diseased mice, suggesting a contribution of disease pathology on NP accumulation at spleen. Findings of decreased NP accumulation in liver and spleen emphasize the role of Mo in off-target tissue accumulation, but also underscore the involvement of other cell types in NP clearance.

Off-target NP accumulation at tissues, such as kidney and lung, are impacted by NP physiochemical properties (i.e., size, surface charge, shape, surface chemistry, etc.). Here, kidney and lung exhibited the most interesting changes in biodistribution after M_{Φ} depletion.^{32,33} Based on our findings of increased kidney biodistribution, it is likely that an inflammatory milieu promoted NP extravasation through leaky vessels due to kidney tubular injury caused by Mφ depletion,³⁴ though kidney Mφ depletion was not directly analyzed in our studies since significant NP kidney accumulation was not observed previously. 18 In the lungs, studies report increased NP accumulation regardless of NP type. ^{7,8} However, NP accumulation in lung is more extensive in epithelial and endothelial cells versus $M\phi$. ³³ In conjunction with our data that show lung M\phi depletion was elusive, it is, therefore, not surprising that CLO treatment did not decrease NP lung accumulation. Increasing NP dose 10-fold in non-depleted mice resulted in significant increases in all off-target organs except for kidneys. At high NP doses, Mφ depletion did not decrease NP accumulation in the liver and spleen, as had been observed in low dose studies, likely due to compensatory uptake of NPs by other cells besides Mφ. Interestingly, NP accumulation in the lung was also unchanged in Mo depleted and saturated conditions, which further supports NP accumulation independent of $M\phi$. Overall, these studies, combined with prior reports, 7,8 emphasize that the

magnitude of accumulation is dependent on injury and/or disease. ^{7,8} Most importantly, the fracture data highlighted the limitations of $M\phi$ depletion and saturation strategies on improving site specific delivery.

The findings that $M\phi$ depletion impacts naı̈ve bone accumulation but not in fractures suggest significant hurdles remain for tissuetargeted DDS: namely, to successfully evade clearance by Mφ. The cascade of events leading up to tissue accumulation involve (a) protein adsorption to DDS, including opsonins, (b) significant phagocytic clearance from circulation, (c) extravasation through leaky vasculature, and, finally, (d) binding to target tissue. 6,35-37 While reducing Mφ and saturating MPS are useful for fundamental investigations, these approaches are not clinically translatable due to risk of immune system compromise, potential off-target toxicities,8 and disruptions in the fracture healing cascade,²⁸ beyond the lack of efficacy observed in these studies. Therefore, further modifications of the TBP-NP platform must be developed such that MPS is avoided, the fracture healing cascade is not impacted, and accessibility of targeting ligands are not compromised. Current approaches to achieve these design criteria include PEGylation and zwitterionic surface chemistries that prolong the circulation time of NPs through Mφ evasion. 38,39 Other notable approaches involve using CD47 mimicking peptides to reduce recognition by $M\phi$. Nevertheless, these $M\phi$ evasive approaches are not without challenges. For example, PEGylation has been associated with complement activation and adverse immune reactions, and can impact target ligand accessibility. 41,42 These limitations motivate fundamental studies, such as those undertaken here, to investigate how MPS interact with various nanomaterials based on material properties and disease/injury type. Though our studies did not definitively identify a route to improve TBP-NP fracture site accumulation due to the relationship of Mφ and targeting epitope (TRAP), the findings inform future design approaches, including Mφ evading functionalities, for the next generation of fracture targeted NPs.

5 | CONCLUSION

MPS was discovered to play a major role in limiting bone delivery efficiency of TRAP binding peptide (TBP)-PSMA-b-PS NPs, despite improved fracture site accumulation. Here, we showed that Mφ were the predominant cells responsible for bone-targeted NP clearance. When Mφ were systemically depleted in uninjured and fractured mice, decreased liver and splenic NP accumulation and increased bone accumulation was observed. Interestingly, there were also increases in lung, kidney, and heart accumulation after reducing Mφ, which suggested compensatory mechanisms of clearance within MPS. When a high dose of TBP-NPs was used to saturate liver MPS, there was a significant increase in NP accumulation in all tissues except for kidneys. These studies confirm the need to develop approaches to evade Mφ to improve delivery efficiency. Furthermore, the circulation time of TBP-NPs and how it relates to tissue accumulation should be investigated to gain a greater appreciation for the DDS, and the lessons learned from this work should be applied for developing other bonetargeted DDS.

ACKNOWLEDGMENTS

The authors gratefully thank Karen Bentley, M.S., (University of Rochester Medical Center Electron Microscopy Shared Laboratory) for EM image acquisition and Dr. James McGrath (University of Rochester) for equipment use. Funding for this study was provided by the National Science Foundation (CBET1450987 (CAREER Award) and DMR2103553 (D.S.W.B.)), National Institutes of Health (NIH) P30 AR069655, R01 AR064200, R01 AR056696 (D.S.W.B.), F31 CA228391 (M.A.F.), University of Rochester CTSA award number UL1 TR002001 (D.S.W.B.), University Research Award (D.S.W.B.) and Drug Discovery Grant (D.S.W.B.).

CONFLICT OF INTEREST

The authors have declared no conflicts of interest for this article.

DATA AVAILABILITY STATEMENT

The data that support the findings of this study are available from the corresponding author upon reasonable request.

ORCID

Marian A. Ackun-Farmmer https://orcid.org/0000-0003-3081-5115

Baixue Xiao https://orcid.org/0000-0001-8337-8401

Maureen R. Newman https://orcid.org/0000-0002-9004-3332

Danielle S.W. Benoit https://orcid.org/0000-0001-7137-8164

REFERENCES

- Bertrand N, Wu J, Xu X, Kamaly N, Farokhzad OC. Cancer nanotechnology: the impact of passive and active targeting in the era of modern cancer biology. *Adv Drug Deliv Rev.* 2014;66:2-25. https://doi.org/10.1016/j.addr.2013.11.009
- Whitehead KA, Langer R, Anderson DG. Knocking down barriers: advances in siRNA delivery. *Nat Rev Drug Discov*. 2009;8(2):129-138. https://doi.org/10.1038/nrd2742
- Anselmo AC, Mitragotri S. Nanoparticles in the clinic: an update. Bioeng Transl Med. 2019;4(3):e10143. https://doi.org/10.1002/btm2. 10143
- Cheng Y-H, He C, Riviere JE, Monteiro-Riviere NA, Lin Z. Meta-analysis of nanoparticle delivery to tumors using a physiologically based pharmacokinetic modeling and simulation approach. ACS Nano. 2020;14(3):3075-3095. https://doi.org/10.1021/acsnano.9b08142
- Wilhelm S, Tavares AJ, Dai Q, et al. Analysis of nanoparticle delivery to tumours. *Nat Rev Mater*. 2016;1(5):1-12. https://doi.org/10.1038/ natrevmats.2016.14
- Blanco E, Shen H, Ferrari M. Principles of nanoparticle design for overcoming biological barriers to drug delivery. *Nat Biotechnol*. 2015; 33(9):941-951. https://doi.org/10.1038/nbt.3330
- Ohara Y, Oda T, Yamada K, et al. Effective delivery of chemotherapeutic nanoparticles by depleting host Kupffer cells. *Int J Cancer*. 2012;131(10):2402-2410. https://doi.org/10.1002/ijc.27502
- Tavares AJ, Poon W, Zhang YN, et al. Effect of removing Kupffer cells on nanoparticle tumor delivery. Proc Natl Acad Sci U S A. 2017;114(51):E10871-E10880. https://doi.org/10.1073/pnas. 1713390114
- Liu T, Choi H, Zhou R, Chen IW. RES blockade: a strategy for boosting efficiency of nanoparticle drug. *Nano Today*. 2015;10(1):11-21. https://doi.org/10.1016/j.nantod.2014.12.003
- Wolfram J, Nizzero S, Liu H, et al. A chloroquine-induced macrophagepreconditioning strategy for improved nanodelivery. *Sci Rep.* 2017;7(1): 13738. https://doi.org/10.1038/s41598-017-14221-2

- Wan Z, Zhao L, Lu F, et al. Mononuclear phagocyte system blockade improves therapeutic exosome delivery to the myocardium. *Theranostics*. 2020;10(1):218-230. https://doi.org/10.7150/thno.38198
- Ellens H, Mayhew E, Rustum Y. Reversible depression of the reticuloendothelial system by liposomes. *Biochim Biophys Acta Gen Subj.* 1982;714 (3):479-485. https://doi.org/10.1016/0304-4165(82)90157-x
- Sun X, Yan X, Jacobson O, et al. Improved tumor uptake by optimizing liposome based RES blockade strategy. *Theranostics*. 2017;7(2):319-328. https://doi.org/10.7150/thno.18078
- Hao J, Han T, Wang M, et al. Temporary suppression the sequestrated function of host macrophages for better nanoparticles tumor delivery. *Drug Deliv*. 2018;25(1):1289-1301. https://doi.org/10.1080/10717544.2018.1474965
- Proffitt RT, Williams LE, Presant CA, et al. Liposomal blockade of the reticuloendothelial system: improved tumor imaging with small unilamellar vesicles. *Science*. 1983;220(4596):502-505. https://doi. org/10.1126/science.6836294
- Ouyang B, Poon W, Zhang YN, et al. The dose threshold for nanoparticle tumour delivery. *Nat Mater*. 2020;19(12):1362-1371. https://doi.org/10.1038/s41563-020-0755-z
- Low SA, Galliford CV, Yang J, Low PS, Kopecek J. Biodistribution of fracture-targeted GSK3beta inhibitor-loaded micelles for improved fracture healing. *Biomacromolecules*. 2015;16(10):3145-3153. https://doi.org/10.1021/acs.biomac.5b00777
- Wang Y, Newman MR, Ackun-Farmmer M, et al. Fracture-targeted delivery of beta-catenin agonists via peptide-functionalized nanoparticles augments fracture healing. ACS Nano. 2017;11(9):9445-9458. https://doi.org/10.1021/acsnano.7b05103
- Baranello MP, Bauer L, Benoit DS. Poly(styrene-alt-maleic anhydride)-based diblock copolymer micelles exhibit versatile hydrophobic drug loading, drug-dependent release, and internalization by multidrug resistant ovarian cancer cells. Biomacromolecules. 2014;15 (7):2629-2641. https://doi.org/10.1021/bm500468d
- Baranello MP, Bauer L, Jordan CT, Benoit DSW. Micelle delivery of parthenolide to acute myeloid leukemia cells. *Cell Mol Bioeng*. 2015;8 (3):455-470. https://doi.org/10.1007/s12195-015-0391-x
- Ackun-Farmmer MA, Soto CA, Lesch ML, et al. Reduction of leukemic burden via bone-targeted nanoparticle delivery of an inhibitor of Cchemokine (C-C motif) ligand 3 (CCL3) signaling. FASEB J. 2021;35(4): e21402. https://doi.org/10.1096/fj.202000938RR
- Newman MR, Russell SG, Schmitt CS, et al. Multivalent presentation of peptide targeting groups alters polymer biodistribution to target tissues. *Biomacromolecules*. 2018;19(1):71-84. https://doi.org/10. 1021/acs.biomac.7b01193
- Ackun-Farmmer MA, Alatise KL, Cross G, Benoit DSW. Ligand density controls C-type lectin-like molecule-1 receptor-specific uptake of polymer nanoparticles. Adv Biosyst. 2020;4:2000172. https://doi.org/ 10.1002/adbi.202000172
- Selander KS, Monkkonen J, Karhukorpi EK, Harkonen P, Hannuniemi R, Vaananen HK. Characteristics of clodronate-induced apoptosis in osteoclasts and macrophages. Mol Pharmacol. 1996;50(5):1127-1138.
- Ehrlich P. Croonian lecture—on immunity with special reference to cell life. Proc R Soc Lond. 1900;66:424-448. https://doi.org/10.1098/ rspl.1899.0121
- Chen KH, Lundy DJ, Toh EK, et al. Nanoparticle distribution during systemic inflammation is size-dependent and organ-specific. *Nanoscale*. 2015;7(38):15863-15872. https://doi.org/10.1039/c5nr03626g
- Sindhwani S, Syed AM, Ngai J, et al. The entry of nanoparticles into solid tumours. *Nat Mater*. 2020;19(5):566-575. https://doi.org/10. 1038/s41563-019-0566-2
- Lin HN, O'Connor JP. Osteoclast depletion with clodronate liposomes delays fracture healing in mice. J Orthop res. 2017;35(8):1699-1706. https://doi.org/10.1002/jor.23440
- Samuelsson E, Shen H, Blanco E, Ferrari M, Wolfram J. Contribution of Kupffer cells to liposome accumulation in the liver. Colloids Surf B

- Biointerfaces. 2017;158:356-362. https://doi.org/10.1016/j.colsurfb. 2017.07.014
- Zhang YN, Poon W, Tavares AJ, McGilvray ID, Chan WCW. Nanoparticle-liver interactions: cellular uptake and hepatobiliary elimination. J Control Release. 2016;240:332-348. https://doi.org/10. 1016/j.jconrel.2016.01.020
- Cataldi M, Vigliotti C, Mosca T, Cammarota M, Capone D. Emerging role of the spleen in the pharmacokinetics of monoclonal antibodies, nanoparticles and Exosomes. *Int J Mol Sci.* 2017;18(6):1249. https://doi.org/10.3390/ijms18061249
- 32. Du B, Yu M, Zheng J. Transport and interactions of nanoparticles in the kidneys. *Nat Rev Mater*. 2018;3(10):358-374. https://doi.org/10.1038/s41578-018-0038-3
- Dhand C, Prabhakaran MP, Beuerman RW, Lakshminarayanan R, Dwivedi N, Ramakrishna S. Role of size of drug delivery carriers for pulmonary and intravenous administration with emphasis on cancer therapeutics and lung-targeted drug delivery. RSC Adv. 2014;4(62): 32673-32689. https://doi.org/10.1039/c4ra02861a
- Kim MG, Su Boo C, Sook Ko Y, et al. Depletion of kidney CD11c+ F4/80+ cells impairs the recovery process in ischaemia/reperfusioninduced acute kidney injury. Nephrol Dial Transplant. 2010;25(9): 2908-2921. https://doi.org/10.1093/ndt/gfq183
- Nel AE, Madler L, Velegol D, et al. Understanding biophysicochemical interactions at the nano-bio interface. *Nat Mater.* 2009;8(7):543-557. https://doi.org/10.1038/Nmat2442
- Tenzer S, Docter D, Kuharev J, et al. Rapid formation of plasma protein corona critically affects nanoparticle pathophysiology. *Nat Nanotechnol*. 2013;8(10):772.
- 37. Xiao W, Gao H. The impact of protein corona on the behavior and targeting capability of nanoparticle-based delivery system. *Int J Pharm.* 2018;552(1–2):328-339. https://doi.org/10.1016/j.ijpharm.2018.10.011
- Moghimi SM, Hunter AC, Murray JC. Long-circulating and targetspecific nanoparticles: theory to practice. *Pharmacol Rev.* 2001;53(2): 283-318.
- Yoo J-W, Chambers E, Mitragotri S. Factors that control the circulation time of nanoparticles in blood: challenges, solutions and future prospects. *Curr Pharm des*. 2010;16(21):2298-2307. https://doi.org/10.2174/138161210791920496
- Rodriguez PL, Harada T, Christian DA, Pantano DA, Tsai RK, Discher DE. Minimal "self" peptides that inhibit phagocytic clearance and enhance delivery of nanoparticles. *Science*. 2013;339(6122):971-975. https://doi.org/10.1126/science.1229568
- Verhoef JJ, Carpenter JF, Anchordoquy TJ, Schellekens H. Potential induction of anti-PEG antibodies and complement activation toward PEGylated therapeutics. *Drug Discov Today*. 2014;19(12):1945-1952. https://doi.org/10.1016/j.drudis.2014.08.015
- Suk JS, Xu Q, Kim N, Hanes J, Ensign LM. PEGylation as a strategy for improving nanoparticle-based drug and gene delivery. Adv Drug Deliv Rev. 2016;99:28-51. https://doi.org/10.1016/j.addr.2015. 09.012

SUPPORTING INFORMATION

Additional supporting information may be found online in the Supporting Information section at the end of this article.

How to cite this article: Ackun-Farmmer, M. A., Xiao, B., Newman, M. R., & Benoit, D. S. W. (2022). Macrophage depletion increases target specificity of bone-targeted nanoparticles. *Journal of Biomedical Materials Research Part A*, 110(1), 229–238. https://doi.org/10.1002/jbm.a.37279